crystal-to-counter distance gave rise to weak measured intensities, because of the significant absorption of the reflected X-rays by the air in the counter arm. For this reason we considered filling the counter arm with hydrogen, but came to the conclusion that a simpler approach would be to make the bulk of the measurements from crystals mounted to rotate about their $[\bar{1}10]$ axes.

In this setting, the pyramidal end of the crystals fitted against the wall of the capillary tube in which they were mounted (Fig. 26.1.2.5*b*). The roughly square cross section of the crystals perpendicular to the rotation axis tended to minimize the absorption variation, which was significant with crystals of linear dimensions of about 0.5 mm. The use of large crystals was necessary with a relatively weak X-ray source running at 800 W and with a foreshortened focal spot of 0.4 × 0.4 mm.

It was convenient to index the reflections in a monoclinic cell, as shown in Fig. 26.1.3.2. In this orientation, the reciprocal lattice presented a diamond pattern to the triple-counter array, whose windows were set parallel to the rotation axis. The reflections therefore occurred in two intersecting sets of levels, the odd and even levels, which had to be measured separately. However, the need to collect alternate levels in this way conferred the advantage that the counters could be positioned closer to the crystal (27.1 cm) than in the *a*-axis mounting so that $>70\%$ of the reflected X-rays were transmitted to the counters. Despite the complexity that this geometry introduced at the data processing and reduction stages, the significant advantages that it offered at the experimental stage ensured its use. The use of a c^* mounting would have been even more advantageous, but it was ruled out both by the difficulty of mounting the crystals in this orientation and by the fact that the counter arm could not be set to the required length of 18.5 cm.

Native data were collected both from crystals rotated about the *a* axis and from crystals rotated about $[\bar{1}10]$ so that they could be scaled together to form a consistent set of three-dimensional data.

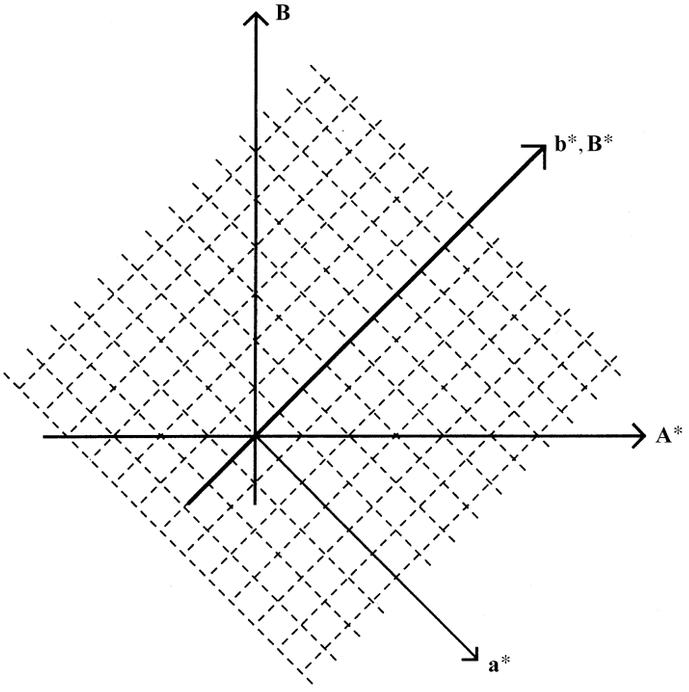

Fig. 26.1.3.2. The a^*b^* plane of the reciprocal lattice oriented to rotate about the $[\bar{1}10]$ axis. The indexing of reflections in a monoclinic unit cell with axes A^* and B^* is also shown. A^* coincides with [110] in the tetragonal lattice and B^* coincides with b^*. The rotation axis is the *B* axis in the monoclinic cell. The reciprocal-lattice dimensions with Cu $K\alpha$ radiation are $a^* = b^* = 0.0195$; $c^* = 0.0406$ r.l.u., while the cell diagonal in the a^*b^* plane is 0.0276 r.l.u.

For the derivatives, however, data were collected only from crystals rotating about their $[\bar{1}10]$ axes and these data were scaled together to form two sets, one comprising levels with odd indices corresponding to the rotation axis and the other with even indices. These measurements, comprising some 1200 reflections, could be made from a single crystal exposed to the X-ray beam for about 20 h. The odd and even data sets for the derivatives were then scaled separately to the native data to give complete sets of three-dimensional data. These low-resolution measurements were made during the first half of 1964 and, after processing by the methods described below, they were used in September 1964 to calculate a new image of the structure at 6 Å resolution.

26.1.3.3. *The second low-resolution map at 6 Å*

Our purpose in calculating a new electron-density map at 6 Å was fourfold. First to ascertain whether the procedures used to identify the five derivatives thought to be satisfactory at this level of resolution had worked satisfactorily. Second, to judge the quality of the measurements made by the triple-counter diffractometer. Third, to explore the effects of the modified method of applying absorption corrections to the intensities that are described below, although these were not expected to have a very great effect at low resolution. Fourth, to examine the effectiveness of the new procedure for incorporating anomalous-scattering information in the phase determination, which is also described below.

Comparison of the two sets of structure amplitudes gave a conventional *R* value of 0.075, which is not particularly good – perhaps because of the comparatively large background values associated with these low-angle measurements. However, the mean figure-of-merit obtained in the new phase calculations was 0.97 as compared with the 0.86 obtained originally. The root-mean-square difference in electron density between the two maps was 0.012 e Å^{-3}, from which it may be judged that the two maps were very similar. Nevertheless, the outline of the molecule was certainly clearer in the new map, and within the molecule there was improved continuity, suggesting the course of a folded polypeptide chain, and there were a number of stronger rod-like features suggestive of α-helices. Two of these were prominent, running upwards from right to left, in the view of the new model shown in Fig. 26.1.3.3.

The result was very encouraging, and we therefore went ahead immediately with data collection at 2 Å resolution, using essentially the same methods. At the same time, we began to plan low-resolution studies of inhibitor binding to lysozyme, from which we hoped to derive information about the nature of the enzyme–substrate complex.

26.1.3.4. *Intensity measurements at high resolution*

At high resolution, measurements were made from only six levels from native crystals set to rotate about the *a* axis while a complete set of data was collected from crystals rotating about $[\bar{1}11]$. As at low resolution, the *a*-axis levels were important for scaling together the odd and even sets of levels measured from crystals rotated about the tetragonal $[\bar{1}11]$ axis. No high-resolution measurements were made from derivative crystals rotated about the *a* axis, the intention being to scale the odd and even subsets of derivative data directly to the native.

26.1.3.4.1. *Experimental methods*

The crystals can be thought of as roughly flattened on $(00\bar{1})$ with liquid between $(00\bar{1})$ and the capillary tube in which they were mounted. In order to minimize the effect of the liquid on absorption, we therefore measured the reciprocal-lattice hemisphere with *C* and c^* positive. Reflections were scanned along *A*, and the origin of the

Copyright © 2006 International Union of Crystallography

scanning slide was offset for upper levels so that, for example, the centre of the scanning slide was the $H = -4$ for the level $K = 8$.

Crystals could be set fairly well by eye. Viewed through the diffractometer microscope, they looked roughly square in the [001] direction, and the arcs of the goniometer head were set so that the edges were horizontal and vertical. When the crystal was turned through 90° from this position, the reflection of a light held level with the microscope could often be seen in the true (110) face. Setting the crystals on the goniometer head with [001] parallel to one of the arcs facilitated subsequent adjustments.

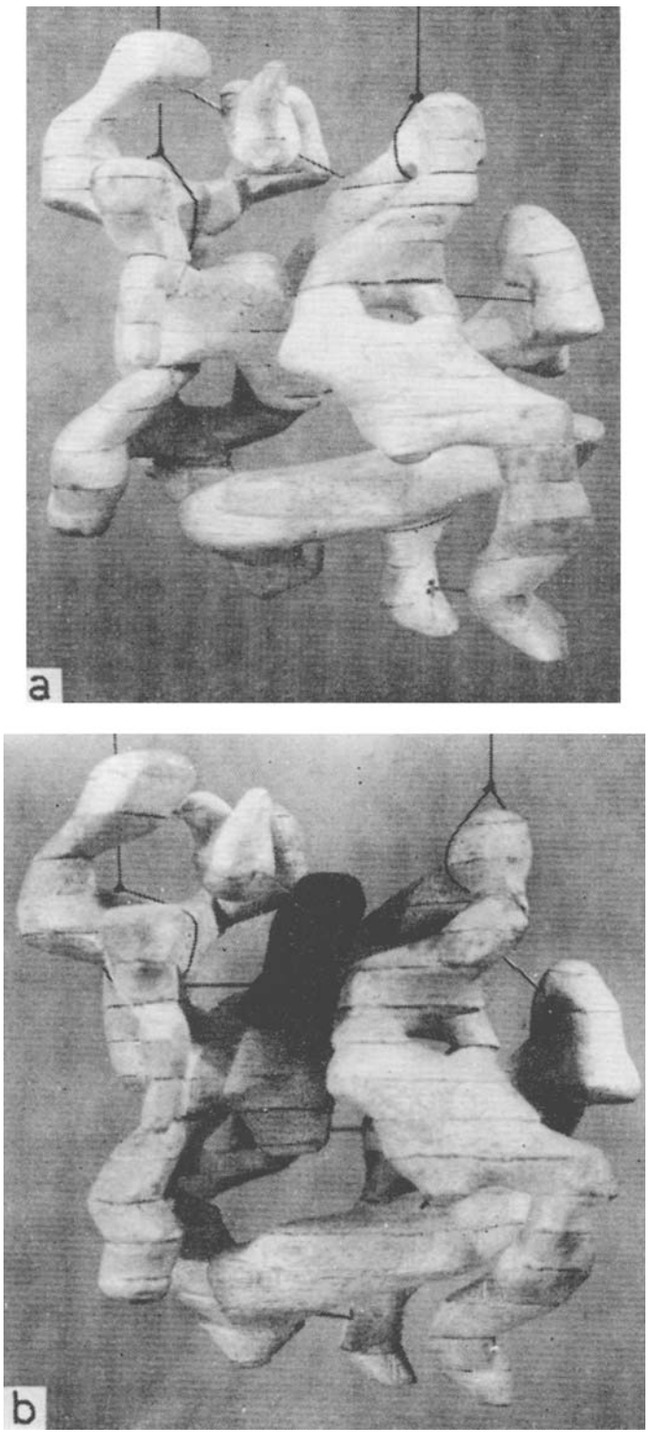

Fig. 26.1.3.3. Solid model of the electron density greater than about 0.5 e Å^{-3} in the second study of lysozyme at 6 Å resolution. This view of the model is equivalent to a view of the original model seen horizontally from the right of Fig. 26.1.2.13(*c*). (*a*) The new model has a marked cleft running roughly vertically down the other side of the model, corresponding to the one that can be seen in Fig. 26.1.2.13(*c*). (*b*) The cleft was shown to bind inhibitor molecules. The black density is that observed for the lysozyme–GlcNAc complex at 6 Å resolution.

Fine adjustment of crystal orientation was achieved by setting on the $\bar{4}40$ reflection. For this purpose, C – the vertical slide – was set to 0.1104 and the inclination angle to $\mu = 3° 5'$. Then, if one arc was set fairly well by eye, the other could be oriented parallel to the incident X-ray beam and adjusted to locate the reflection. The two arcs were then adjusted in turn to give the optimum setting, in which the crystal was rotated about the normal to the ($\bar{4}40$) plane.

The orientation in the AC reciprocal-lattice plane was determined by returning the vertical slide to zero and setting the upper (scanning) slide to 0.1104 with the lower (stepping) slide at zero. The crystal was then rotated until the monoclinic 400 reflection appeared. At this stage, checks were made with the top/bottom and left/right slits to make sure that the crystal was well centred in the X-ray beam and that the counter apertures were well positioned. Similar checks were made with the crystal rotated about 180° to the monoclinic $\bar{4}00$ reflection.

The final check on crystal orientation was to locate the 008 reflection near 0.3248 on the lower (stepping) slide, with the other slides set at zero. There was some variation in the value of c^* for different crystals, and c^* was often closer to 0.0404 than to 0.0406 r.l.u.

At this stage, the first measurements were made of the intensities of the reflections (monoclinic) 400, 16,0,0 and 008. These reference reflections were remeasured at intervals during the measurement of each triplet of reciprocal-lattice levels as a check on the stability of the whole system and irradiation damage to the crystal. The measurements were manually entered on the diffractometer output tape and monitored by the data-processing program.

In order to set the diffractometer for a particular triplet of levels, we found it convenient to leave the lower slide set for the 008 reflection, to adjust the vertical slide and the tilt angle (μ) for the levels in question, and then to run out along the stepping slide until a suitable high-angle reflection was found. The crystal rotation angle was then optimized for this reflection.

Finally, careful checks were made to ensure that the reflections to be measured fell in the reciprocal-lattice hemisphere with L positive, and that they were indexed in a right-handed axial system. The automatic run was then begun at the 2 Å limit on the stepping (C^*) slide, and all reflections were scanned from H_{max} to $-H_{max}$ on the scanning slide. Virtually all reflections within (and in some directions a little beyond) the 2 Å limit were measured in this way in fourteen triplet levels, seven even and seven odd. About 2000 reflections were measured in a typical overnight run, and data collection for each species of crystal took slightly more than two weeks.

The derivative crystals required for these measurements were prepared by the diffusion method described above, and about 20 of them were mounted at the same time at the beginning of the data-collection process to ensure that they were all the same. At the end of a run, careful measurements were made of the peak intensity of the $\bar{4}40$ reflection as the crystal was rotated through steps of 15° about the crystal-mounting axis (φ). These measurements were used during data processing in an improved method of absorption correction devised by North *et al.* (1968).

26.1.3.4.2. *Diffractometer output*

The output from the triple-counter diffractometer again consisted of a plain-language output for immediate checking of the results and output at this stage on eight-hole-punched paper tape for immediate

references